Journal of Natural Gas Science and Engineering 82 (2020) 103506

Contents lists available at ScienceDirect

Journal of Natural Gas Science and Engineering

journal homepage: http://www.elsevier.com/locate/jngse

Effects of CH_4–CO_2 replacement in hydrate-bearing sediments on S-wave velocity and electrical resistivity

Jongwon Jung [a], Jae Eun Ryou [a], Riyadh I. Al-Raoush [b], Khalid Alshibli [c], Joo Yong Lee [d,*]

[a] School of Civil Engineering, Chungbuk National University, Cheongju-si, Chungbuk, 28644, South Korea
[b] Department of Civil & Architectural Engineering, Qatar University, P.O Box 2713, Doha, Qatar
[c] Department of Civil and Environmental Engineering, The University of Tennessee, Knoxville, TN, 37996, USA
[d] Petroleum and Marine Research Division, Korea Institute of Geoscience and Mineral Resources, Daejeon, South Korea

A B S T R A C T

CH_4–CO_2 replacement has been considered as a method for methane production from hydrate-bearing sediments to maintain sediment stability. Sediment stability has been studied at both the particle scale and mesoscale. However, the shear stiffness of sediments has not yet been explored. Moreover, the effects of CO_2 and CO_2–N_2 mixtures as injection fluids on sediment stability remain unclear. Thus, this study aimed to determine the variations in shear wave velocity and electrical resistivity during hydrate formation, CH_4–CO_2 replacement, and hydrate dissociation using two types of injecting fluids (CO_2 and CO_2–N_2 mixture). The results demonstrated that hydrate-bearing sediment could maintain its stability during CH_4–CO_2 replacement by injecting CO_2 or CO_2–N_2 mixture. Furthermore, injecting CO_2–N_2 mixture was more efficient for methane production than injecting CO_2. The Results also revealed that injecting CO_2–N_2 mixture could lead to higher stability of sediments during CH_4–CO_2 replacement than injecting CO_2, although the difference in sediment stability was small between the two cases.

1. Introduction

CH_4 hydrate is a potential energy resource with worldwide reserves on the order of 500–10,000 Gt of carbon (Collett, 2002; Kvenvolden, 1988; Milkov, 2004; Ruppel and Pohlman, 2008). Depressurization, heating, and chemical injection have been used for methane production from hydrate-bearing sediments. Injecting CO_2 into hydrate-bearing sediments can produce methane. CO_2 is not only a gas that can be used for methane production but also a gas that causes global warming. Fortunately, CO_2 can be sequestrated as CO_2 hydrate in sediments (McGrail et al., 2007; Ota et al., 2005; Stevens et al., 2008; Svandal et al., 2006; Zhou et al., 2008; Jung et al., 2010). Chemical potential difference between CO_2 and CH_4 hydrate can result in CH_4–CO_2 replacement in hydrate (Seo and Lee, 2001; Svandal et al., 2006). CH_4–CO_2 replacement is affected by pressure and temperature-dependent relative viscosity, permeability, density, and solubilities of water, CH_4, and CO_2 (Jung et al., 2010). Previous studies on the CH_4–CO_2 replacement ratio or rate demonstrate that the CH_4–CO_2 replacement rate can increase close to the CH_4 hydrate phase boundary and with injected CO_2 gas pressure until CO_2 is liquefied (McGrail et al., 2007; Ota et al., 2005, 2007). The replacement ratio also increases when CO_2/N_2 mixture is used as the injecting fluid. This is because smaller N_2 molecules can replace CH_4 in small cages (Park et al., 2006). The chance of reaction between the CH_4 hydrate and injected CO_2 increases with slower injection of CO_2 and longer soaking time of CO_2, which in turn increases the replacement ratio (Seo et al., 2015, 2016).

CH_4–CO_2 replacement by injecting CO_2 into hydrate-bearing sediments can maintain the stability of sediments during methane production (Jung and Santamarina 2010; Espinoza and Santamarina, 2010). Although the replacement ratio and rate have been well studied, the stability of hydrate-bearing sediment during and after CH_4–CO_2 replacement has not been well understood yet. Previous studies have shown no change in electrical conductivity and stiffness of hydrate during CH_4–CO_2 replacement in particle scale using electrodes and the change in amplitude of P-waves (Jung and Santamarina 2010), constant P-wave velocity during CH_4–CO_2 replacement in sediments (Espinoza and Satamarina 2011), and decreased electrical conductivity in sediments (Lim et al., 2017). These results show that the stability of hydrate-bearing sediments could be maintained during CH_4–CO_2 replacement. However, the extent to which stability could be maintained is unclear. Therefore, this limits the utilization of the CO_2 injection method for the production of methane from hydrate-bearing sediments in the field. Thus far, no study has considered the measurement of S-wave velocity during CH_4–CO_2 replacement. Also, no study has reported the different effects of CO_2 and CO_2–N_2 mixtures as an injecting fluid on the stability and shear wave velocity during CH_4–CO_2

* Corresponding author.
E-mail address: jyl@kigam.re.kr (J.Y. Lee).

https://doi.org/10.1016/j.jngse.2020.103506
Received 10 April 2020; Received in revised form 15 June 2020; Accepted 22 July 2020
Available online 30 July 2020

replacement in hydrate-bearing sediments. Shear wave velocity has a strong correlation with sediment shear stiffness and shear strength. Thus, the objectives of this study were to determine the S-wave velocity and electrical resistance of hydrate-bearing sediments during CH_4–CO_2 replacement and to investigate the stability of hydrate-bearing sediment using two types of injecting fluids (i.e., CO_2 and CO_2–N_2 mixture) at core scales.

2. Experimental setup

2.1. Materials

Ottawa sand #20–30 was used as the host sediment ($d_{50} = 0.72$ mm, $d_{60}/d_{10} = 1.2$). CH_4 gas with a purity of 99.95 mol % was used for CH_4 hydrate formation. CO_2 gas with a purity of 99.995 mol % and N_2/CO_2 mixed gas (20 mol % CO_2 with N_2 balance, 99.995 mol % purity) were used for comparison with the results. NaCl aqueous solution (3.35 wt %) was used to synthesize CH_4 hydrate formation to mimic the natural environment.

2.2. Experimental setup

Fig. 1 shows a schematic diagram of the experimental setup. A high-pressure system was designed for the CH_4–CO_2 replacement tests. (1) A back-pressure regulator (BPR, TESCOM 26-1765-24, Emerson Electric Co., Elk River, MN) was used to maintain the maximum internal pressure during continuous CO_2 injection. (2) A mass flow controller (MFC, Brooks 5850E, Hatfield, PA) was used to maintain a constant flow rate during CO_2 injection. (3) A wet gas meter (WGM, W-NK-1, Shinagawa Co., Ltd., Japan) was used to measure the volume of CH_4 and CO_2 gases when the CH_4–CO_2 mixture flowed out from the main chamber during the tests. (4) A gas chromatograph (GC, YL-6100, Young Lin Instrument Co., Ltd., Republic of Korea) was used for the quantitative analysis of guest compositions of the synthesized gas hydrates. (5) A pressure transducer (Omega PX303-GV) and (6) thermocouples (T-types) were used to monitor pressure and temperature changes during the tests, respectively. (7) A data logger recorded the variations in pressure and temperature. (8) A syringe pump controlled the pressure in the entire system. (9) Bender elements and electrodes were placed in the sediments and were used to measure the shear wave velocity and electrical resistance during the tests. (10) A Teflon spacer with epoxy resin was used for electrical insulation of the system, and (11) the source bender element was connected to a signal generator that sent a step function signal every 20 ms. The receiver bender element was connected to a pre-amplifier and a digital storage oscilloscope.

2.3. Experimental procedures

Water-saturated (NaCl aqueous solution) sand was packed inside the sediment cell with a target initial porosity of 39% for both tests (Table 1).

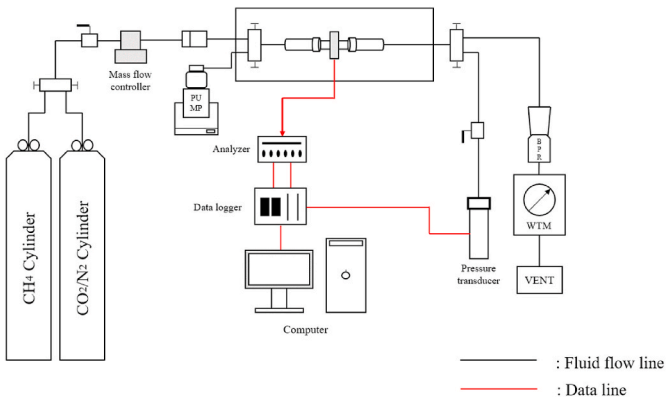

Fig. 1. Schematic drawing of the experimental setup.

The sediment cell was placed inside the high-pressure chamber and flushed five times with nitrogen gas to reach irreducible water saturation conditions. Then, the temperature was lowered to 263 K for ice formation (Fig. 2a) and maintained for 100–400 s. The temperature was then increased to 276 K to melt the ice (Fig. 2b). Then, CH_4 was introduced into the sediments while keeping the pressure and temperature constant at ~9 MPa and 276 K, respectively, within the CH_4 hydrate stability field (Fig. 2c). The CH_4 hydrate started to nucleate. Pressure and temperature were maintained constant for 24 h to allow CH_4 hydrate formation and growth in the sediments. Then, the hydrate saturation was calculated using Equation (1) [Sakamoto et al., 2005]. After the CH_4 hydrate formation was complete, liquid CO_2 (or CO_2–N_2 mixture) was injected into the pore space of the sediment at a constant flow rate (100 sccm, standard cubic centimeters per minute) to displace CH_4 in the pore space, while the pressure was maintained at 9 MPa using a back pressure regulator (BPR) at the outlet (Fig. 2d). CO_2 (CO_2–N_2 mixture) and CH_4 gases were produced, and their composition was measured using gas chromatography (GC). The injection of liquid CO_2 (or CO_2–N_2 mixture) into the sediment continued until the CH_4 composition of the outlet gas was less than 1 mol %. After completing the CH_4–CO_2 replacement, the pressure was decreased in three steps: (1) from liquid CO_2 to gas CO_2 (Fig. 2e), (2) between the CH_4 and CO_2 stability fields (i.e., outside the CH_4 hydrate stability field but within the CO_2 hydrate stability field) (Fig. 2f), and (3) outside the CO_2 hydrate stability field (Fig. 2g).

$$S_{hyd}(\%) = \frac{V_{wd}\Delta p T_0}{172 p_0 T_f A_{beads} L_{beads} \varphi} \times 100, \quad (1)$$

where V_{wd} is the volume of water drained by the injected gas; Δp is the pressure drop in the sediment cell during hydrate formation; T_o is the standard temperature; 172 is the ideal volume ratio of stored methane per hydrate; p_o is the standard pressure; T_f is the temperature during hydrate formation; A is the cross-sectional area of the sediment; L is the length of the sediment; and φ is the porosity of the porous media.

2.4. Measurement of electrical resistivity and shear wave velocity

Electrical resistance and shear wave velocity were measured for each step of CH_4 hydrate formation, CH_4–CO_2 replacement, and the dissociation of CO_2 hydrate during pressure decrease. The errors for electrical resistivity and shear wave velocity were ±0.001 Ωm and ±0.1 m/s, respectively.

The electrical resistivity of the gas hydrate was measured using two stainless steel plate electrodes. The cross-sectional area (A) of the electrodes was 0.785 cm^2, while the distance between the two electrodes was 1.55 cm. Electrical resistivity was measured with an electrical interface device (SI 1287 and SI 1260, Solartron Analytical, U.K.). The voltage was 0.1 V to minimize electrode polarization and electrochemical reactions on the electrodes during measurement. The electrical resistivity (ρ) was calculated using the measured electrical resistance, according to Equation (2).

$$\rho = \beta \frac{A}{L} R, \quad (2)$$

where β is the shape factor ($\beta = 1$ for a simple cylindrical shape), A is the

Table 1
Experimental conditions.

Porosity [%]	Irreducible water saturation [%]	Hydrate saturation [%]	Injecting fluid types
39	44	22	CO_2/N_2
39	43	21	CO_2

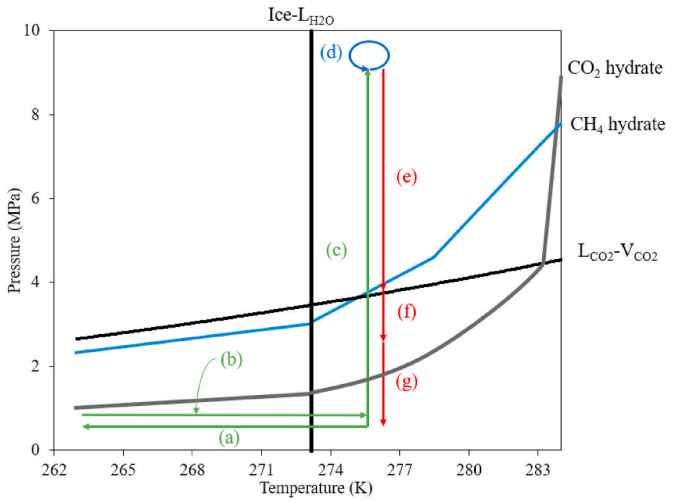

Fig. 2. Changes in pressure and temperature for CH_4 hydrate formation, CH_4–CO_2 replacement, and hydrate dissociation. The labels in the figure denote the following: (a) temperature decrease to form ice, (b) temperature increase in melting the ice, (c) pressure increase to form methane hydrate, (d) CO_2 (or CO_2/N_2 mixture) injection for CH_4–CO_2 replacement, (e) pressure decrease from liquid CO_2 to gas CO_2 zone, (f) pressure decrease from CH_4 hydrate stability zone to CO_2 hydrate stability zone, and (g) pressure decrease out of CO_2 hydrate stability zone.

cross-sectional area of the gas hydrate-bearing sediment in the sediment cell, and L is the distance between the two electrodes.

Shear wave velocity was estimated from the arrival time of the first signal and the distance between two bender elements. The source bender element transmitted a step function signal every 20 ms. The receiver bender element was connected to a pre-amplifier and a digital storage oscilloscope to monitor the signal passing through the sediment. The shear wave velocity was associated with hydrate saturation in Equation (3) and the shear modulus, as shown in Equation (4).

$$V_{s\_hbs}^2 = \alpha\left(\frac{\sigma_{\parallel}^{'} + \sigma_{\perp}^{'}}{2kPa}\right)^{\beta} + \left(\frac{V_h S_h^2}{n}\right)^2 \theta, \tag{3}$$

where σ′ is the effective stress in the direction of wave propagation, S_h is the hydrate saturation, V_h is the shear-wave velocity of pure hydrate, and θ is the hydrate formation type (e.g., cementing or pore-filling). Parameter α is the shear-wave velocity at 1 kPa mean stress. Parameter β is the sensitivity of velocity to the state of stress, which can be estimated from tests conducted on sediments without hydrates. The presence of hydrates in sediments increased the stiffness of both the pore fluid and sediment skeleton. As shown in Equation (4), skeletal stiffening influenced the increase in shear modulus, thus increasing the skeletal bulk modulus.

$$K_{sk} = \frac{2(1+v_{sk})}{3(1-2v_{sk})} G. \tag{4}$$

Moreover, the shear modulus is related to the S-wave velocity in Equation (5), where ρ is the mass density of the medium.

$$V_s = \sqrt{\frac{G}{\rho}}. \tag{5}$$

3. Results and discussion

The multi-stage tests to explore the effects of injected gas (CO_2 or CO_2–N_2 mixture) on the stability of hydrate-bearing sediments during CH_4–CO_2 replacement yielded two results.

3.1. Electrical resistivity and shear wave velocity during CH_4 hydrate formation

After the sediment cell inside the high-pressure chamber was flushed with nitrogen, sediment reached irreducible water saturation (43–44%) (Table 1). The results (Fig. 3) show the variations in electrical resistivity and shear wave velocity at the irreducible water saturation condition of the experiments as a function of CH_4 pressure before hydrate formation. Both electrical resistivity and shear wave velocity exhibited relatively constant values (i.e., electrical resistivity and shear wave velocity were 0.41–0.43 Ω and 248–250 m/s, respectively). Note that the errors for electrical resistivity and shear wave velocity were ±0.001 Ωm and ±0.1 m/s, respectively. The results of shear wave velocity (i.e., 248–250 m/s) without hydrates in sediment, in this study, are consistent with Santamarina (2001), implying that gas pressure does not influence the stiffness of the sediments. Moreover, when water saturation was in the range of 43–44%, the results of electrical resistivity (i.e., 0.41–0.43Ω) in sediments were consistent with those presented by Lim et al., (2017).

As shown in Fig. 4, CH_4 hydrate formation resulted in a decrease in pressure due to the consumption of methane during CH_4 hydrate formation. The estimated hydrate saturation was 21%−22% in the two tests, as calculated based on the degree of pressure drop using Equation (1). Table 1 provides a summary of all the experimental results. The results (Fig. 4) also show that the electrical resistivity increased between 29.1 and 32.0 Ω during CH_4 hydrate formation, which is consistent with Lim et al., (2017). Moreover, the results show that higher hydrate saturation (i.e., 22%) caused higher electrical resistivity (i.e., 32.0 Ω) in the two tests. This is because more hydrate formation consumed more water in the pores, thus causing water content to decrease.

In agreement with Jung et al., (2012), the results (Fig. 4) show that shear wave velocity increased during CH_4 hydrate formation. Moreover, higher hydrate saturation resulted in a higher shear wave velocity. Hydrate saturation, could also be estimated using Equation (4), which is a function of the shear wave velocity for different effective stress levels (Jung et al., 2012). The parameters, α = 80 m/s and β = 0.25, were selected for hydrate-free sand. In contrast, Vh = 1964 m/s was obtained from the literature (Koh et al., 2012). According to Santamarina and Ruppel (2008), the value of θ ranges from 0.08 to 0.25. In this study, the effective stress was close to zero. When the value of θ was assumed to be 0.25, the estimated hydrate saturation, *Sh*, was 48%, which was higher than the value obtained with Equation (1) (i.e., 21–22%). This finding implies that the estimation of hydrate saturation using Equation (3) is not accurate when the effective stress is zero.

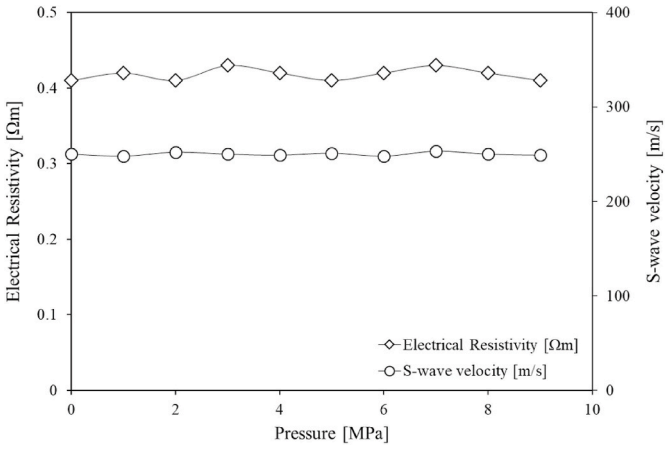

Fig. 3. Electrical resistivity and shear wave velocity measurement of irreducible water saturation in sediments as a function of CH_4 pressure.

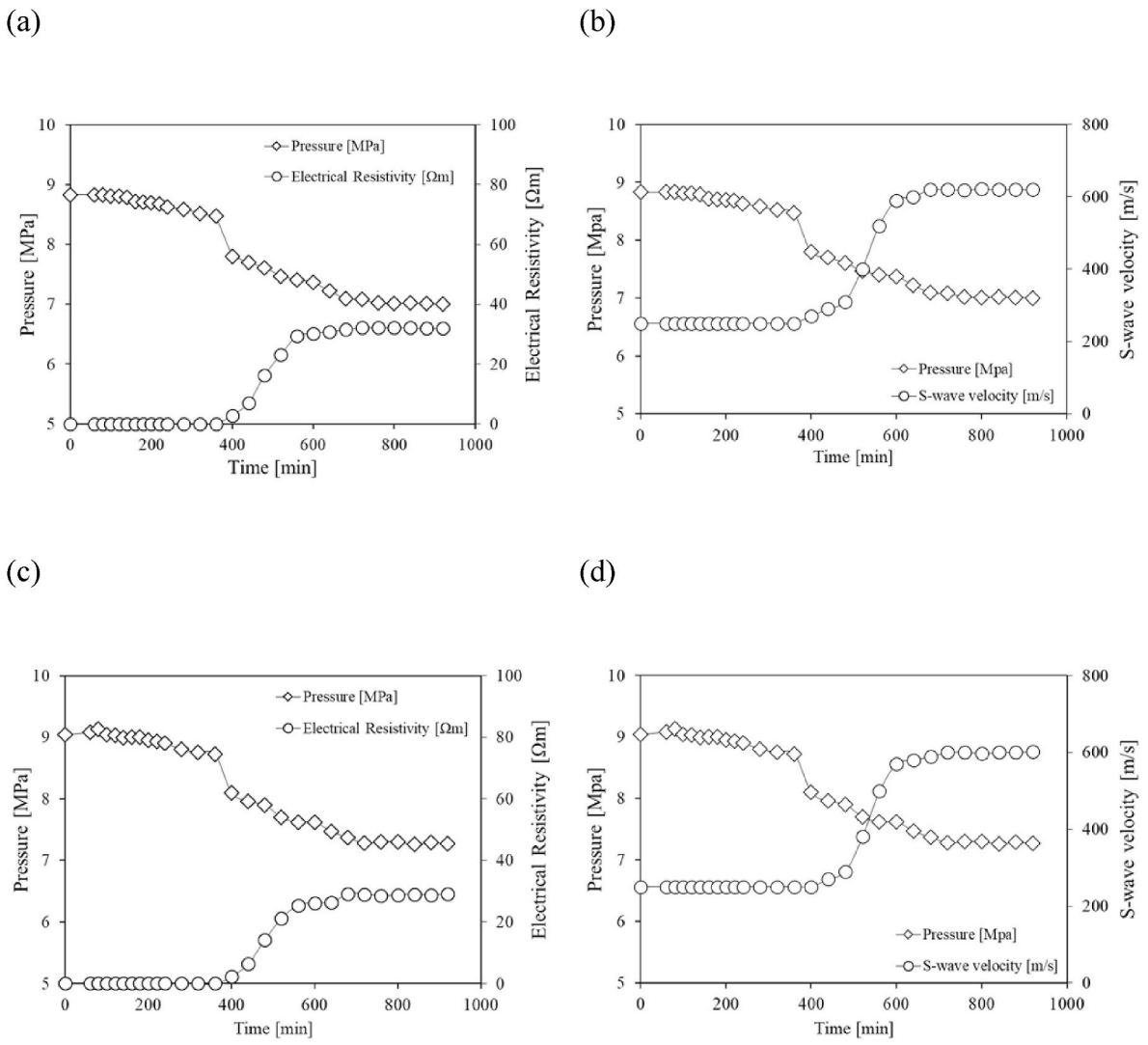

Fig. 4. Pressure, electrical resistivity, and S-wave velocity change during CH_4 hydrate formation. (a) Changes in pressure and electrical resistivity during hydrate formation for CO_2–N_2 injection; (b) Changes in pressure and S-wave velocity during hydrate formation for CO_2–N_2 injection; (c) Changes in pressure and electrical resistivity during hydrate formation for CO_2 injection; and (d) Changes in pressure and S-wave velocity during hydrate formation for CO_2 injection.

3.2. Electrical resistivity and shear wave velocity during CH_4–CO_2 replacement

CO_2 and CO_2–N_2 mixtures (80 mol % N_2 balanced with CO_2) were injected into the sediments containing CH_4 hydrate at a constant flow rate of 100 sccm for a continuous replacement process. As soon as the CO_2/CO_2–N_2 mixture was injected, the electrical resistivity decreased (see Fig. 5). Momentary dissociation at the interface by contact between the injected gas (CO_2 or CO_2–N_2 mixture) and the hydrate surface may result in an immediate change in electrical resistivity (Lim et al., 2017). The electrical resistivity after CO_2–N_2 mixture injection was approximately 12 Ω. Note that the error of the electrical resistivity is ±0.001 Ωm. This finding implies that ~40% of CH_4 was replaced with a CO_2–N_2 mixture according to a previous study (Lim et al., 2017). The electrical resistivity (i.e., ~10 Ω) after CO_2 injection may also present less CH_4–CO_2 replacement (i.e., less than 40%) relative to CO_2–N_2 mixture injection (Lim et al., 2017). These results are consistent with previous studies that showed that the replacement ratio increased with increasing CO_2–N_2 mixture due to smaller N_2 molecules that could replace CH_4 in small cages (Park et al., 2006).

The shear wave velocity in both tests increased after CO_2 (or CO_2–N_2 mixture) injection (see Fig. 7). When the CO_2–N_2 mixture was injected, the shear wave velocity (i.e., ~640 m/s) was relatively faster when compared to post CO_2 injection. Note that the error of the shear wave velocity is ±0.1 m/s. In agreement with Park et al., (2006), this finding implies that further CH_4–CO_2 replacement occurred after injection of the CO_2–N_2 mixture than when CO_2 was injected due to small N_2 molecules.

3.3. Electrical resistivity and shear wave velocity during and after hydrate dissociation

After completion of the CH_4–CO_2 replacement, the pressure was decreased through three steps. First, the pressure was decreased from 9.1–9.2 MPa–3.5 MPa, while the temperature was maintained at 276 K (Fig. 6). The PT condition was located between the phase boundaries of liquid CO_2 and gas CO_2. During this step, no changes were observed in the electrical resistivity or shear wave velocity. Second, the pressure was decreased from 3.5 MPa to 2.5 MPa, while the temperature was maintained at 276 K (Fig. 6). The PT condition was located between the phase boundaries of CO_2- and CH_4 hydrates, which was out of the CH_4 hydrate phase but inside the CO_2 hydrate phase. Thus, CH_4 hydrate could not remain in this PT condition (see Fig. 2e). The results showed that the electrical resistivity increased, but the shear wave velocity decreased during the second step because about 40% replacement occurred during

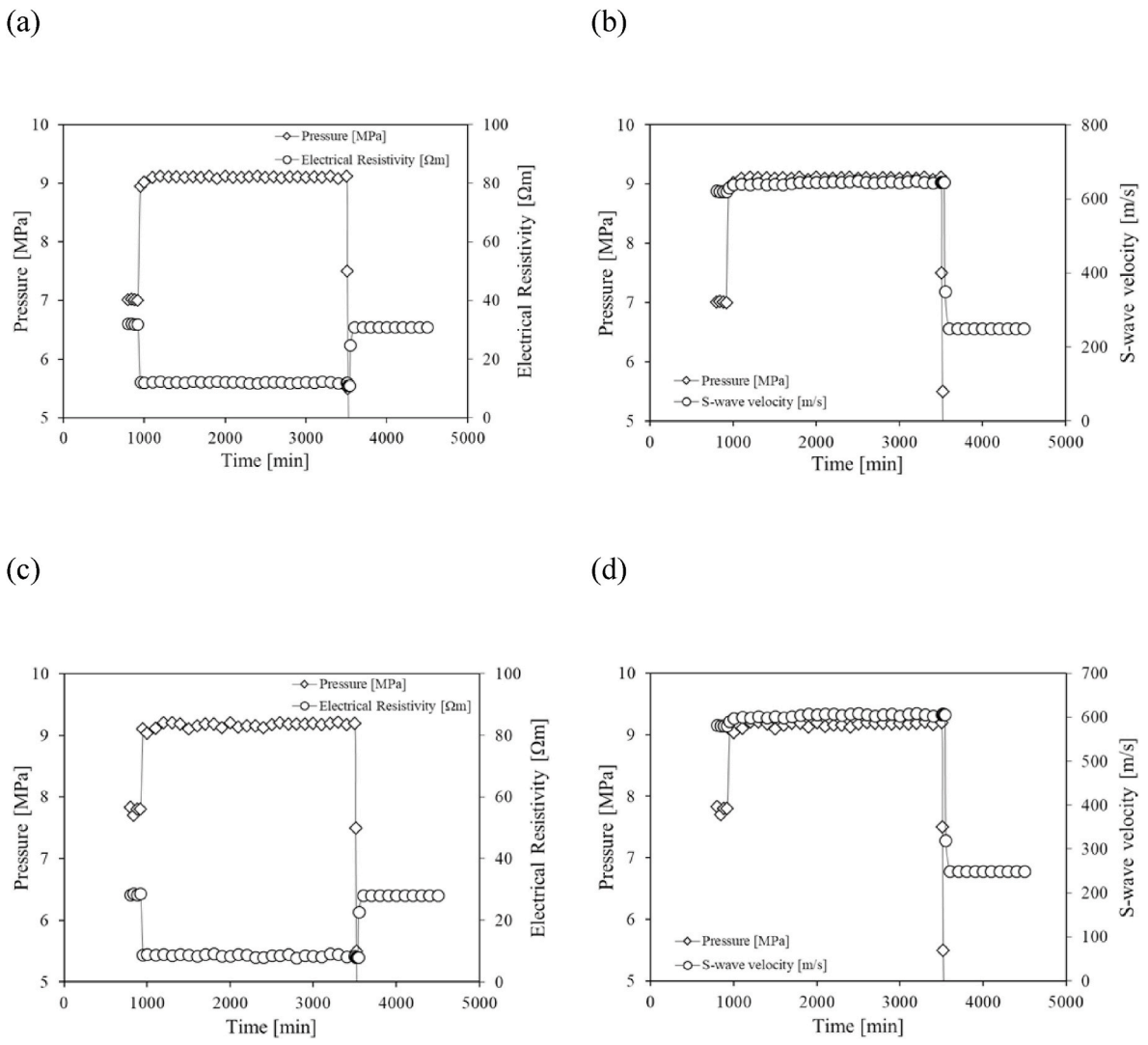

Fig. 5. Pressure, electrical resistivity, and S-wave velocity change during CH_4–CO_2 replacement. (a) Changes in pressure and electrical resistivity during hydrate formation for CO_2–N_2 injection; (b) Changes in pressure and S-wave velocity during hydrate formation for CO_2–N_2 injection; (c) Changes in pressure and electrical resistivity during hydrate formation for CO_2 injection; and (d) Changes in pressure and S-wave velocity during hydrate formation for CO_2 injection.

CO_2 or CO_2–N_2 mixture, which caused CH_4 hydrate to remain in the sediments and the remaining CH_4 hydrate dissociated (Fig. 6). When the CO_2–N_2 mixture was injected, a smaller amount of CH_4 hydrate remained. Thus, variations in electrical resistivity and shear wave velocity were lower with the injection of the CO_2–N_2 mixture than with CO_2 injection. This finding implies that the injection of the CO_2–N_2 mixture could be a more stable method when the pressure decreases during and after CH_4–CO_2 replacement.

Third, the pressure decreased outside the CO_2 hydrate phase boundary, while the temperature remained relatively constant (see Fig. 2f). The pressure was decreased by less than 1.7 MPa, while the temperature was maintained at 276 K (Fig. 6). During this step, the electrical resistivity increased, but the shear wave velocity decreased to initial values before hydrate formation. This finding implied that the displaced CO_2 hydrate became dissociated in the sediment (Fig. 6).

4. Discussion

Two types of gases (i.e., pure CO_2 and CO_2–N_2 mixture) were injected into CH_4 hydrate-bearing sediments for CH_4–CO_2 replacement. The results showed that when a CO_2–N_2 mixture was injected, a higher replacement ratio (i.e., a 38% replacement ratio with a CO_2–N_2 mixture and 28% with pure CO_2) resulted in more CO_2 replacement in the small cages in the hydrate due to the small molecule size of N_2. This finding implies that injecting CO_2–N_2 can produce more CH_4 under the same conditions. In both tests, the S-wave velocity increased while electrical resistivity decreased during CH_4–CO_2 replacement, implying that the stability of sediments could be maintained. It is known that a CO_2–N_2 mixture can result in higher replacement efficiency owing to the smaller molecule size of N_2. The results also indicated that sediments maintained higher stability when CO_2–N_2 mixture is injected because the S-wave velocity is higher when CO_2–N_2 is injected. This finding implies that using a CO_2–N_2 mixture could lead to better stability and replacement efficiency than using only CO_2.

5. Conclusion

It is known that hydrate-bearing sediments can maintain their stability during and after CH_4–CO_2 replacement. However, the effects of injected fluids (i.e., CO_2 or CO_2–N_2 mixture) on the stability of sediments remain unclear. Thus, this study investigated the effects of two types of fluids on the stability of sediments during CH_4–CO_2 replacement. The following conclusions are drawn from this study:

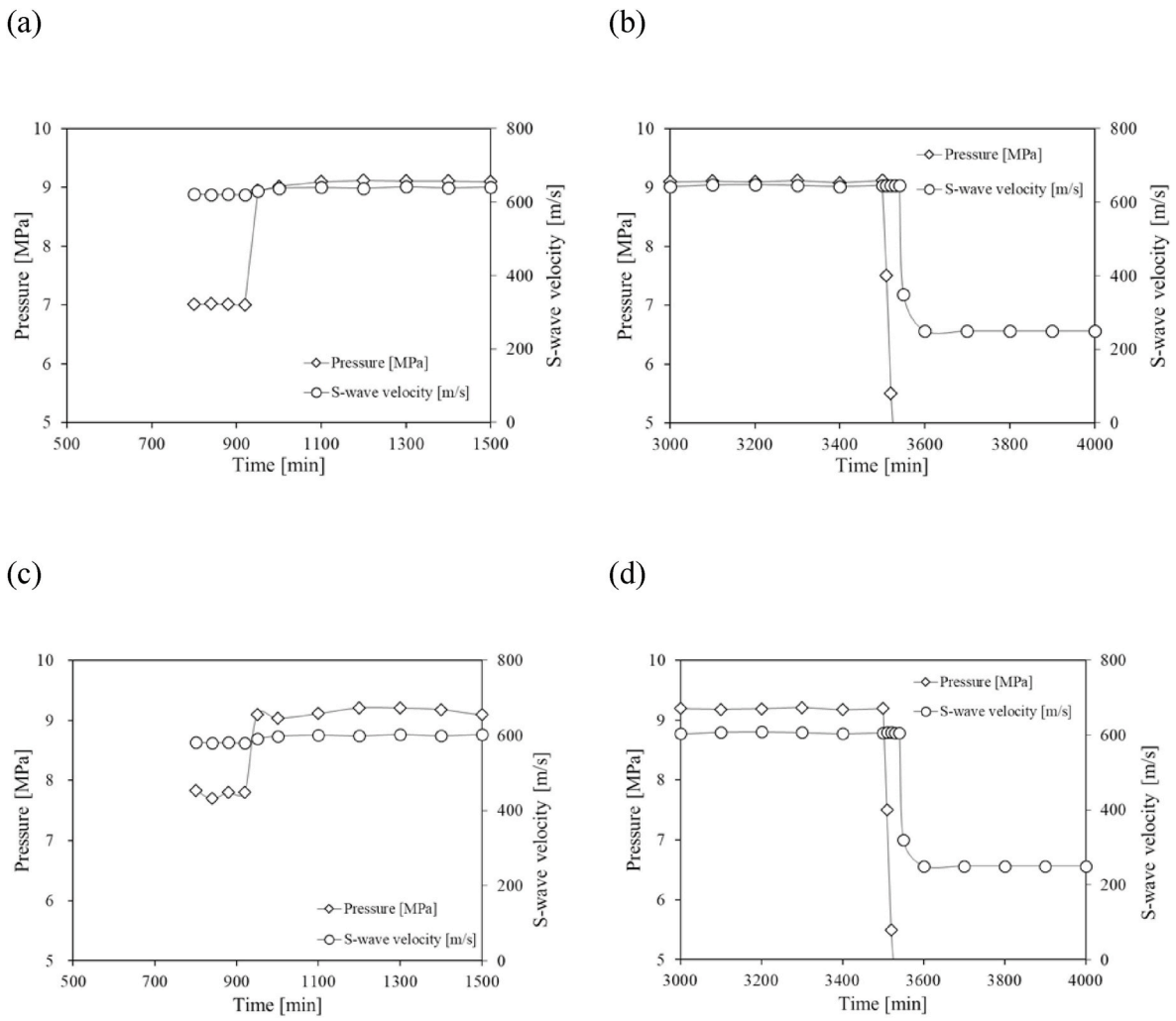

Fig. 6. Pressure, electrical resistivity, and S-wave velocity change during pressure drop. (a) Changes in pressure and electrical resistivity during hydrate formation for CO_2–N_2 injection; (b) Changes in pressure and S-wave velocity during hydrate formation for CO_2–N_2 injection; (c) Changes in pressure and electrical resistivity during hydrate formation for CO_2 injection; and, (d) changes in pressure and S-wave velocity during hydrate formation for CO_2 injection.

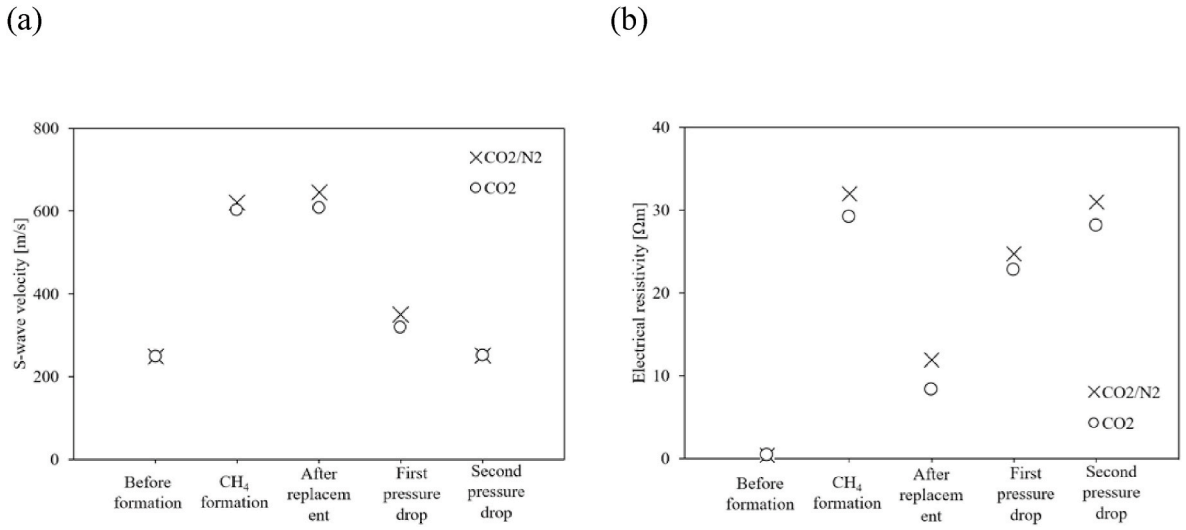

Fig. 7. S-wave velocity and electrical resistivity change in all procedures. (a) Changes in S-wave velocity during the whole procedures for CO_2–N_2 and CO_2 injection; and (b) changes in electrical resistivity during the whole procedures for CO_2–N_2 and CO_2 injection.

- Gas pressure does not influence the stiffness of the sediments. Neither electrical resistivity nor shear wave velocity is influenced by the change in pressure before hydrate formation in sediments.
- Electrical resistivity increases with CH_4 hydrate formation due to increased stiffness of sediments and decreased water content. Moreover, the shear wave velocity increases with CH_4 hydrate formation due to increased stiffness of sediments.
- As soon as the CO_2/CO_2–N_2 mixture is injected into CH_4 hydrate-bearing sediments, momentary dissociation at the interface by contact between the injected gas (CO_2 or CO_2–N_2 mixture) and the hydrate surface occurs, which results in an immediate decrease in electrical resistivity. However, the S-wave velocity increases during CO_2/CO_2–N_2 mixture injection. This implies that the stability of sediments can be maintained during CH_4–CO_2 replacement.
- When the pressure decreases from liquid CO_2 to the gaseous CO_2 PT zone, neither electrical resistivity nor shear wave velocity changes, thus implying no change in sediment stiffness.
- When the PT condition is located between the CH_4 hydrate and CO_2 hydrate phase boundary, the electrical resistivity increases. However, the shear wave velocity decreases because the remaining CH_4 hydrate dissociates. As PT conditions move outside the CO_2 hydrate phase boundaries, the electrical resistivity significantly increases while the shear wave velocity decreases.
- Injecting a CO_2–N_2 mixture can produce more CH_4 under the same conditions than injecting CO_2 alone, thus leading to higher stability during CH_4–CO_2 replacement.

CRediT authorship contribution statement

Jongwon Jung: Conceptualization, Methodology, Writing - original draft, Project administration, Funding acquisition. **Jae Eun Ryou:** Investigation, Visualization, Formal analysis. **Riyadh I. Al-Raoush:** Funding acquisition, Project administration, Conceptualization, Writing - review & editing, Data curation, Resources. **Khalid Alshibli:** Formal analysis, Methodology. **Joo Yong Lee:** Conceptualization, Validation, Writing - review & editing, Supervision, Funding acquisition.

Declaration of competing interest

The authors declare that they have no known competing financial interests or personal relationships that could have appeared to influence the work reported in this paper.

Acknowledgement

This research was mainly supported by NPRP grant #NPRP8-594-2-244 from the Qatar National Research Fund (a member of the Qatar Foundation). This research was partially supported by the Ministry of Trade, Industry, and Energy (MOTIE) through the Project “Gas Hydrate Exploration and Production Study (20–1143)” under the management of the Gas Hydrate Research and Development Organization (GHDO) of Korea and the Korea Institute of Geoscience and Mineral Resources (KIGAM). This research is also supported by “Study on Submarin Active Faults and Evaluation of Possibility of Submarine Earthquakes in the Southern Part of the East Sea, Korea (20–9850)” of the Ministry of Ocean and Fisheries. The findings achieved herein are solely the responsibility of the authors.

Appendix A. Supplementary data

Supplementary data to this article can be found online at https://doi.org/10.1016/j.jngse.2020.103506.

References

Collett, T.S., 2002. Energy resource potential of natural gas hydrates. AAPG Bull. 86, 1971–1992.

Espinoza, D.N., Santamarina, J.C., 2010. Water-CO_2-mineral systems: interfacial tension, contact angle, and diffusion—implications to CO_2 geological storage. Water Resour. Res. 46, W07537. https://doi.org/10.1029/2009WR008634.

Espinoza, D.N., Santamarina, J.C., 2011. P-wave monitoring of hydrate-bearing sand during CH4–CO2 replacement. Int. J. Greenh. Gas Contr. 5, 1031–1038. https://doi.org/10.1016/j.ijggc.2011.02.006.

Jung, J.W., Santamarina, J.C., 2010. CH_4-CO_2 replacement in hydrate-bearing sediments: a pore-scale study. G-cubed 11 (12), 2–8.

Jung, J.W., Espinoza, D.N., Santamarina, J.C., 2010. Properties and phenomena relevant to CH_4-CO_2 replacement in hydrate bearing sediments. J. Geophys. Res. 115, B10102.

Jung, J.W., Santamarina, J.C., Soga, K., 2012. Stress-strain response of hydrate-bearing sands: numerical study using discrete element method simulations. J. Geophys. Res. 117, B04202.

Koh, C.A., Sum, A.K., Sloan, E.D., 2012. State of art: natural gas hydrates as a natural resource. J. Nat. Gas Sci. Eng. 8, 132–138, 0.

Kvenvolden, K.A., 1988. Methane hydrate-A major reservoir of carbon in the shallow geosphere? Chem. Gelo. 71, 41–51.

Lim, D., Ro, H., Seo, Y., Seo, Y.J., Lee, J.Y., Kim, S.J., 2017. Thermodynamic stability and guest distribution of CH_4/N_2/CO_2 mixed hydrates for methane hydrate production using N_2/CO_2 injection. J. Chem. Thermodyn. 106, 16–21.

McGrail, B.P., Schaef, H.T., White, M.D., Zhu, T., Kulkami, A.S., Hunter, R.B., Patil 334, S.L., Owen, A.T., Martin, P.F., 2007. Using Carbon Dioxide to Enhance Recovery of 335 Methane from Gas Hydrate Reservoirs: Final Summary Report. PNNL 17035. Pacific 336 Northwest National Laboratory Operated by. Battelle Memorial Institute for the U.S. 337 Department of Energy, Oak Ridge, TN.

Milkov, A.V., 2004. Global estimates of hydrate-bound gas in marine sediments: how much is really out there? Earth Sci. Rev. 66, 183–197.

Ota, M., Morohashi, K., Abe, Y., Watanabe, M., Smith, R.L., Inomata, H., 2005. Replacement of CH_4 in the hydrate by use of liquid CO_2. Energy Convers. Manag. 46, 1680–1691.

Ota, M., Saito, T., Aida, T., Watanabe, M., Sato, Y., Smith, R.L., Inomata, H., 2007. Macro and microscopic CH_4-CO_2 replacement in CH^4 hydrate under pressurized CO_2. AIChE J. 53, 2715–2721.

Park, Y., Kim, D.Y., Lee, J.W., Huh, D.G., Park, K.P., Lee, J., Lee, H., 2006. Sequestering carbon dioxide into complex structures of naturally occurring gas hydrates. Proc. Natl. Acad. Sci. Unit. States Am. 103, 12690–12694.

Ruppel, C.D., Pohlman, J.W., 2008. Climate Change and the Global Carbon Cycle: Perspectives and Opportunities, Fire in the Ice: Methane Hydrate Newsletter, Winter, pp. 5–8.

Sakamoto, Y., Komai, T., Haneda, H., Tenma, N., Yamaguchi, T., 2005. Experimental Study on Modification of Permeability in a Methane Hydrate Reservoir and Gas Production Behavior by the Simultaneous Injection of Nitrogen, the 5th International Conference on Gas Hydrates. Torndheim, Normay.

Santamarina, J.C., Ruppel, C., 2008. The impact of hydrate saturation on the mechanical, electrical, and thermal properties of hydrate-bearing sand, silts, and clay. In: Paper Presented at 6th International Conference on Gas Hydrates, Vancouver, Canada, 6-10 Jul.

Santamarina, J.C., Klein, K.A., Fam, M.A., 2001. Soils and Waves—Particulate Materials Behavior, Characterization and Process Monitoring. Wiley, New York.

Seo, Y.J., Kim, D., Koh, D.Y., Lee, J.Y., Ahn, T., Kim, S.J., Lee, J., Lee, H., 2015. Soaking process for the enhanced methane recovery of gas hydrates via CO_2/N_2 gas injection. Energy Fuels 29, 8143–8150.

Seo, Y.J., Park, S., Kang, H., Ahn, Y.H., Lim, D., Kim, S.J., Lee, J., Lee, J.Y., Ahn, T., Seo, Y., Lee, H., 2016. Isostructural and cage-specific replacement occurring in sII hydrate with external CO_2/N_2 gas and its implications for natural gas production and CO_2 storage. Appl. Energy 178, 579–586.

Seo, Y.T., Lee, H., 2001. Multiple phase equilibria of the ternary carbon dioxide, methane, and water mixtures. J. Phys. Chem. B 105, 10084.

Stevens, J.C., Howard, J.J., Baldwin, B.A., Ersland, G., Husebo, J., Graue, A., 2008. 356 experimental hydrate formation and gas production scenarios based on CO2 357 sequestration. In: Proceedings of the 6th International Conference on Gas Hydrates 358 (ICGH8), Vancouver, BC, Canada, July 6−10, pp. 1–12.

Svandal, A., Kvamme, B., Gràànàsy, L., Pusztai, T., Buanes, T., Hove, J., 2006. The phase-field theory applied to CO_2 and CH_4 hydrate. J. Cryst. Growth 287 (2), 486–490.

Zhou, X., Fan, S., Liang, D., Du, J., 2008. Determination of appropriate condition on replacing methane from hydrate with carbon dioxide. Energy Convers. Manag. 49 (8), 2124–2129.